Developmental Biology 399 (2015) 249–262

Contents lists available at ScienceDirect

Developmental Biology

journal homepage: www.elsevier.com/locate/developmentalbiology

Lizard tail regeneration: regulation of two distinct cartilage regions by Indian hedgehog

Thomas P. Lozito, Rocky S. Tuan*

Center for Cellular and Molecular Engineering, Department of Orthopaedic Surgery, University of Pittsburgh School of Medicine, Pittsburgh, PA, United States

ARTICLE INFO

Article history:
Received 14 September 2014
Received in revised form
18 November 2014
Accepted 31 December 2014
Available online 14 January 2015

Keywords:
Lizard
Cartilage
Regeneration
Indian hedgehog
Growth plate
Ossification
Calcification
Perichondrium

ABSTRACT

Lizards capable of caudal autotomy exhibit the remarkable ability to "drop" and then regenerate their tails. However, the regenerated lizard tail (RLT) is known as an "imperfect replicate" due to several key anatomical differences compared to the original tail. Most striking of these "imperfections" concerns the skeleton; instead of the vertebrae of the original tail, the skeleton of the RLT takes the form of an unsegmented cartilage tube (CT). Here we have performed the first detailed staging of skeletal development of the RLT CT, identifying two distinct mineralization events. CTs isolated from RLTs of various ages were analyzed by micro-computed tomography to characterize mineralization, and to correlate skeletal development with expression of endochondral ossification markers evaluated by histology and immunohistochemistry. During early tail regeneration, shortly after CT formation, the extreme proximal CT in direct contact with the most terminal vertebra of the original tail develops a growth plate-like region that undergoes endochondral ossification. Proximal CT chondrocytes enlarge, express hypertrophic markers, including Indian hedgehog (Ihh), apoptose, and are replaced by bone. During later stages of tail regeneration, the distal CT mineralizes without endochondral ossification. The sub-perichondrium of the distal CT expresses Ihh, and the perichondrium directly calcifies without cartilage growth plate formation. The calcified CT perichondrium also contains a population of stem/progenitor cells that forms new cartilage in response to TGF-β stimulation. Treatment with the Ihh inhibitor cyclopamine inhibited both proximal CT ossification and distal CT calcification. Thus, while the two mineralization events are spatially, temporally, and mechanistically very different, they both involve Ihh. Taken together, these results suggest that Ihh regulates CT mineralization during two distinct stages of lizard tail regeneration.

Introduction

As reptiles, lizards are positioned evolutionarily between amphibians and mammals, and their regenerative potential reflects this. Amphibians, specifically the urodeles (newts and salamanders), are able to regenerate tails and limbs. Lizards are able to regenerate their tails only, and mammals can regenerate neither tails nor limbs. (Note: Not all lizards are able to regenerate their tails. Here, lizards will refer to autotomous, regenerative lizards.) Furthermore, lizards are more closely related to mammals, both of which are classified as amniotes, and, therefore, fundamentally different in terms of life cycle and development from the anamniote, amphibian urodeles. Thus, the lizard is an amniote with developmental processes similar to that of mammals, and, hence, represents a more suitable model than the salamander model to investigate the biology of tissue regeneration (Alibardi, 2010).

Lizard tail regeneration is especially interesting in terms of cartilage regeneration. Urodeles regenerate tissues as near perfect replicas of the originals. The regenerated lizard tail (RLT), however, is known as an "imperfect replicate" due to several key anatomical differences (Bellairs and Bryant, 1985; Alibardi, 2010; Fisher et al., 2012). Most striking of these "imperfections" concerns the skeleton, which is cartilaginous in the RLT. The spinal column and vertebrae of the original tail are regenerated as a single, unsegmented cartilage tube (CT). Unique in the animal kingdom, the lizard CT is an adult organ that only exists in regenerated tissues and is maintained for the duration of the lizard's life without transitioning to bone.

The ability of the CT to resist ossification becomes even more interesting and counterintuitive considering the role cartilage typically plays in bone development. During vertebrate limb development, and during tail and limb regeneration in urodeles, bone is formed from cartilage intermediates in a process known as endochondral ossification (Iten and Bryant, 1976; Kronenberg,

* Correspondence to: Center for Cellular and Molecular Engineering, Department of Orthopaedic Surgery, 450 Technology Drive, Room 221, Pittsburgh, PA 15219 United States. Fax: +412 624 5544.
E-mail address: rst13@pitt.edu (R.S. Tuan).

http://dx.doi.org/10.1016/j.ydbio.2014.12.036
0012-1606/

2003; Mackie et al., 2008). This well-studied process begins with mesenchymal cells condensing to from a cartilage anlage or template. As the mesenchymal cells differentiate into chondrocytes, they proliferate and begin to deposit cartilage extracellular matrix high in collagen type II (Col2) and sulfated glycosaminoglycans (GAGs) (DeLise et al., 2000; Tsang et al., 2014). Stratification of chondrocytes in various states of maturity causes formation of the growth plate, in which the most mature cells cease proliferating and undergo hypertrophy. This critical milestone in the process of endochondral ossification is typified by characteristic changes in chondrocyte morphology, including dramatic increases in cell volume, and a defined gene expression profile (Man-Ger Sun and Beier, 2014). Hypertrophic chondrocytes begin to produce a very specialized matrix consisting of collagen type X (Col10) and express alkaline phosphatase (Alk Phos), and matrix calcification is initiated (Adams et al., 2007; van der Eerden et al., 2003; Anderson et al., 2004). The hypertrophic chondrocytes also begin secreting growth factors such as bone morphogenetic protein 6 (BMP-6) and vascular endothelial growth factor (VEGF) (Zelzer et al., 2001), which induces blood vessels to sprout from the surrounding tissues. The hypertrophic chondrocytes then undergo apoptosis and are replaced by mesenchymal cells and pre-osteoblasts brought into the cartilage template through invading capillaries (Dirckx et al., 2013; Mackie et al., 2008). The remnant cartilage matrix is further cleared by invading cathepsin K-positive osteoclasts and replaced with bone matrix as mesenchymal cells differentiate into osteoblasts. Endochondral ossification concludes when the growth plate closes and the cartilage template is replaced by bone.

The behavior of growth cartilage chondrocytes is exquisitely regulated by environmental signals as they proceed through differentiation, maturation, hypertrophy, and apoptosis. One of the most important factors in regulating endochondral ossification is the molecule Indian hedgehog (Ihh), which has been called a master regulator of embryonic skeletal development (Kronenberg, 2003). Ihh is secreted by pre-hypertrophic chondrocytes as they leave the proliferative pool and, upon binding to its receptor Patched-1 (PTCH-1), activates signaling cascades that activate the expression of a number of factors, including parathyroid hormone-related peptide (PTHrP) (Adams et al., 2007; Chung et al., 2001; Lanske and Kronenberg, 1998; Vortkamp et al., 1996; St-Jacques et al., 1999). PTHrP signals through its receptor, parathyroid hormone receptor-1 (PTHR1), which is expressed at higher levels by hypertrophic chondrocytes than in proliferating chondrocytes. PTHrP signaling prevents chondrocytes from undergoing hypertrophy by keeping them in the proliferative pool (Lee et al., 1996; Kronenberg, 2006; Ohba and Chung, 2014). As the bone develops and lengthens, PTHrP produced at the ends of bones no longer reaches distant chondrocytes, which stop proliferating, undergo hypertrophy, and begin secreting Ihh. Thus, a feedback loop arises in which Ihh secreted in the hypertrophic zone signals back to apical cartilage regions to express PTHrP, thereby controlling the regions in which chondrocytes undergo hypertrophy and terminal differentiation.

The roles of these molecules in lizard tail regeneration have not been studied, and lizards are predisposed to forming cartilage that resists complete calcification and ossification. The peculiarities in skeletal development make the lizard CT without equivalent among animal models. Here we have performed the first detailed staging of skeletal development of the lizard (*Anolis sagrei*) regenerate, with special attention paid to factors known to regulate endochondral ossification. To elucidate the roles and mechanisms of several of these factors, lizard CTs were manipulated with treatments known to be either stimulatory or inhibitory to embryonic cartilage development. The cellular and molecular features here support developing the regenerated lizard tail as a novel experimental model of cartilage regeneration.

Results

The terminal vertebra of the original tail-stump is remodeled prior to autotomy

To analyze mineralization within the RLT, it became critical to accurately distinguish between original and regenerated tail skeletal elements. Thus, we began our study by characterizing the changes that occur within the original tail-stump following autotomy. Each vertebra of the original tail is separated from one another by dorsal zygapophysial joints (Z-joints) (Fig. 1A, B) and ventral intervertebral pads (IPs) (Fig. 1A, C). Like the tails of most autotomous lizards, the original *Anolis* tail exhibits intravertebral fracture planes, preformed breaks in the bone approximately halfway through each vertebrae (Fig. 1A, D, E). During autotomy, the tail separates along a fracture plane, and the tail-stump of a recently autotomized lizard tail ends with a half vertebra (Fig. 2A). A clot immediately forms over the stump, and, by two days post-autotomy (DPA), the stump tissues contract, causing the distal portion of the autotomized half-vertebra to protrude (Fig. 2B). Cathepsin K-positive osteoclasts begin to accumulate at

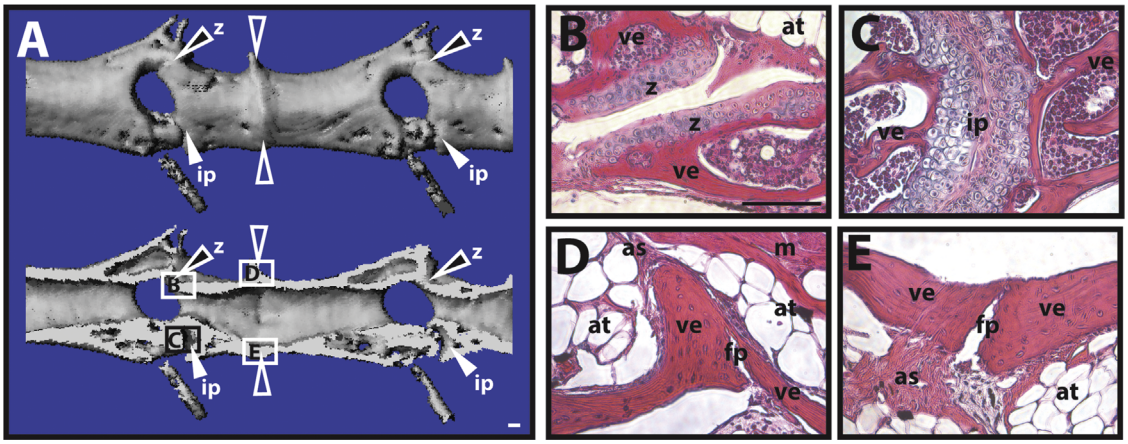

Fig. 1. The vertebrae of the original tail contain fracture planes. (A) Unsectioned (top) and sagittally sectioned (bottom) views of the same portion of original lizard tail analyzed by microCT. Open arrowheads denote intravertebral fracture plane. White-filled arrowheads mark intervertebral pads (ip). Black-filled arrowheads identify Z-joints (z). (B-E) Histological analysis (H&E) of (B) Z-joint, (C) intervertebral pad, and (D, E) fracture plane regions identified in Panel A. at, adipose tissue; as, autotomy septum; fp, fracture plane; m, muscle; ve, vertebra. Bar = 100 μm.

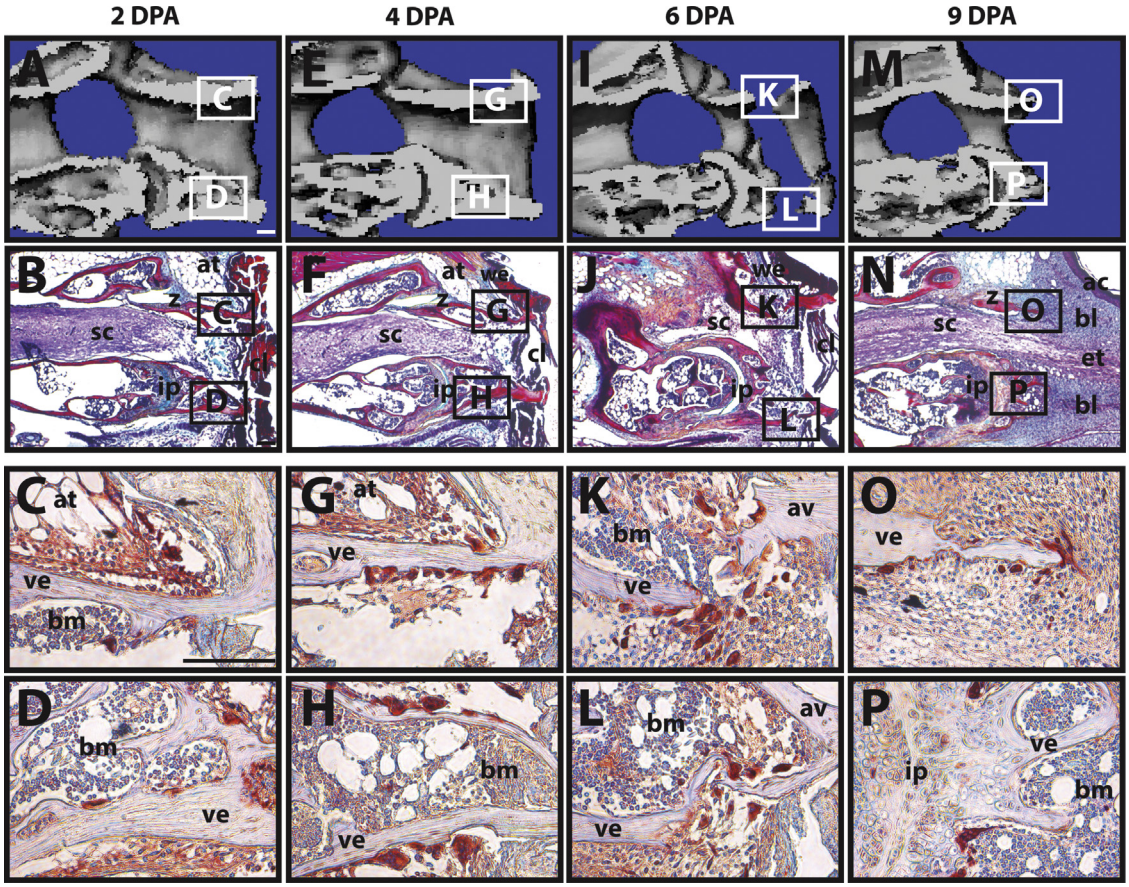

Fig. 2. Osteoclasts remodel the terminal vertebra of the original tail-stump. (A, E, I, M) Sagittally sectioned microCT scans of original tail terminal vertebrae 2, 4, 6, and 9 days post-autotomy (DPA). (B, F, J, N) Histological analysis (Movat's pentachrome) of the same regions depicted in microCT scans. (C, D, G, H, K, L, O, P) Closer views of regions identified in microCT and histology panels analyzed by cathepsin K IHC. Cathepsin K-positive osteoclasts (red) are observed degrading the distal portion of the terminal vertebra. ac, apical cap; at, adipose tissue; av, ablated vertebra; bl, blastema; bm, bone marrow; cl, clot; et, ependymal tube; ip, intervertebral pad; m, muscle; sc, spinal cord; ve, vertebra; we, wound epithelium; z, zygapophysial joint. Bar=100 μm.

the terminal vertebra (Fig. 2C, D). By 4 DPA, the terminal vertebra (Fig. 2E) begins to remodel. Wound epidermis migrates across the autotomized surface beneath the scab until it reaches the protruding half-vertebra (Fig. 2F), and osteoclasts degrade the distal half vertebra (Fig. 2G, H). By 6 DPA, the protruding portion of half-vertebra is separated from the rest of the tail skeleton (Fig. 2I, J) by osteoclast activity (Fig. 2K, L) and is shed along with the scab in a process known as ablation. By 9 DPA, the terminal vertebra has almost completely degraded (Fig. 2M, N), and osteoclastic activity continues until only the IP and Z-joint remain (Fig. 2O, P). Meanwhile, following ablation, the wound epidermis thickens into an apical cap (AC) (Fig. 2N), and the ependymal lining of the original spinal cord elongates toward the AC, forming the ependymal tube (ET) (Fig. 2N). A structure resembling a blastema forms as a mass of proliferating mesenchymal-like cells derived from the tissues of the stump that collect and proliferate around the ET between the IP and the AC (Fig. 2N). Until this point, known as the latent period, very little additional length has been added to the stump, but our findings show that a number of important skeletal changes have taken place. (Note: We, like others (Alibardi, 2010; Delorme et al., 2012; McLean and Vickaryous, 2011), use the term "blastema" loosely in the context of lizard tail regeneration, as there exist important differences between the lizard tail blastema and the classic blastema observed in salamander limb regeneration. Many of these differences concern the positioning of proliferative cells relative to the AC, vascularity, and the identity, origin, and differentiation state of the cells that give rise to the regenerated tissues (Cox, 1969; Hutchins et al., 2014). Furthermore, the term "blastema" is also used to describe early regenerative stages in other species and tissues. For example, the blastema formed during mammalian digit regeneration is reported to depend on a resident stem cell population with the nail bed (Lehoczky et al., 2011), suggesting yet another variation on the classic blastema. Thus, the specifics of blastema formation and composition are probably both tissue and species specific, and while here we refer to the earliest stages of lizard tail regeneration as a blastema, we acknowledge that future studies may redefine this structure.)

We have described four stages based on skeletal development within the *Anolis* regenerated lizard tail following the latent period. These are summarized in Table 1 and are described in greater detail in Supplementary Material (Figs. S1-S5).

The proximal CT develops a growth plate-like structure and undergoes endochondral ossification

During early (Stage 1) RLT skeletal development, blastema cells differentiate into chondrocytes, forming the CT. The proximal CT makes contact with the original lizard tail skeleton at the IP and Z-joint of the terminal vertebra (Fig. 3A, B). No portion of the early CT is mineralized (Fig. 3B), but by 21 DPA the chondrocytes at the extreme proximal CT in contact with the terminal vertebra enlarge (Fig. 3C) and express hypertrophic chondrocyte markers Alk Phos (Fig. 3D) and BMP-6 (Fig. 3E). The CT edges adjacent to these proximal hypertrophic chondrocytes express Ihh (Fig. 3F). By 35 DPA (early Stage 2), this region of hypertrophic chondrocytes expands as the proximal CT develops a growth-plate like organization (Fig. 4A).

Table 1
Summary of stages of regenerated lizard tail skeletal development.

Stage Number	Approximate Time Span	Milestones
1	10–28 DPA	• CT develops • Proximal CT chondrocytes undergo hypertrophy • Proximal CT perichondrium expresses Ihh
2	28–42 DPA	• Ossification centers form between original and regenerated tail skeletons • Proximal CT undergoes endochondral ossification
3	42–70 DPA	• Distal CT perichondrium expresses Ihh • Distal perichondrium calcifies directly
4	After 70 DPA	• CT assumes mature structure • No further mineralization takes place

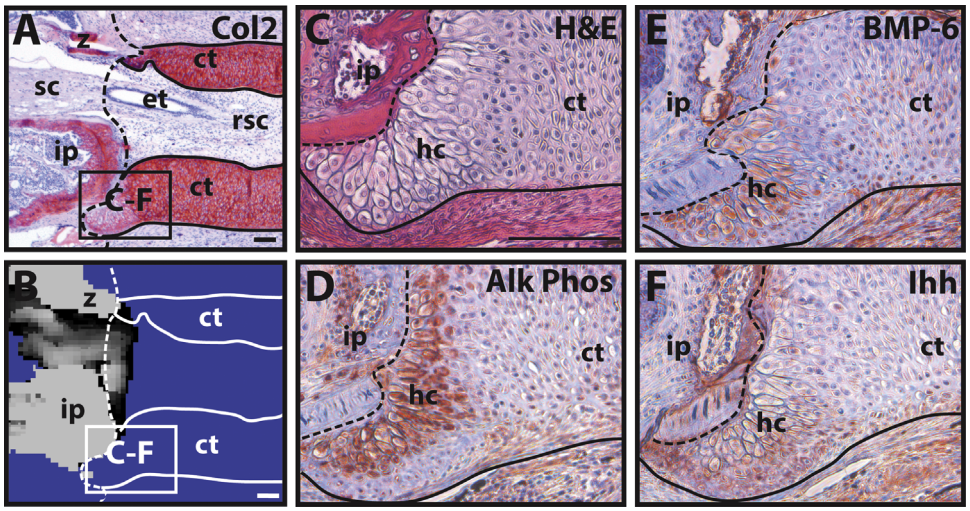

Fig. 3. Proximal CT chondrocytes undergo hypertrophy. (A, B) Sagittally sectioned boundary region between original and regenerated tail (21 DPA) analyzed by (A) Col2 IHC and (B) microCT. Solid line denotes the cartilage tube (CT) boundary. Dashed line denotes the boundary between original (left) and regenerated (right) tail. Chondrocytes near the boundary between original and regenerated tail take on a hypertrophic morphology. (C-F) Higher magnification views of regions identified in Panels A and B analyzed by (C) histological staining (H&E) and IHC for (D) Alk Phos, (E) BMP-6, and (F) Ihh. ct, cartilage tube; et, ependymal tube; hc, hypertrophic chondrocyte region; ip, intervertebral pad; rsc, regenerated spinal cord; sc, spinal cord; z, zygapophysial joint. Bar = 100 μm.

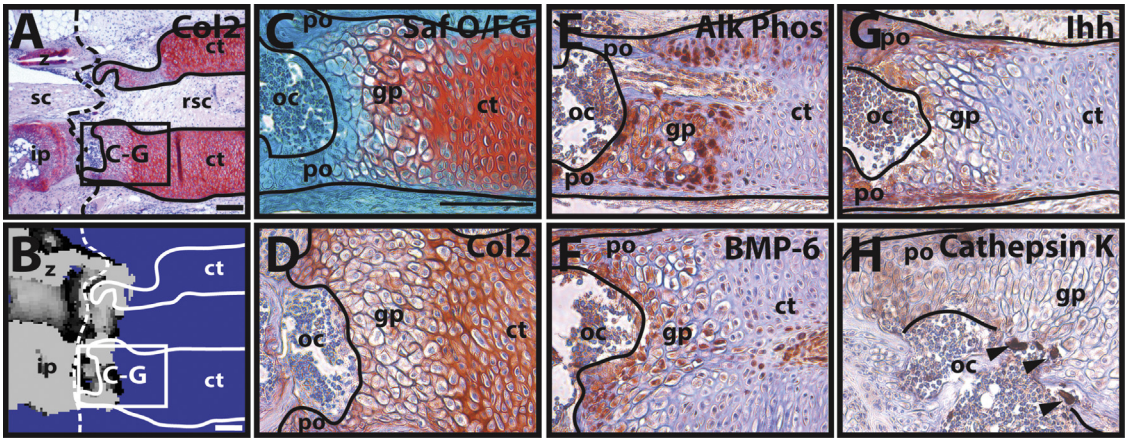

Fig. 4. The proximal CT mineralizes through an endochondral ossification-like process. (A, B) Sagittally sectioned boundary region between original and regenerated tail (35 DPA) analyzed by (A) Col2 IHC and (B) microCT. Solid line denotes the CT boundary. Dashed line denotes boundary between original (left) and regenerated (right) tail. The proximal CT develops a growth plate-like structure. (C-H) Higher magnification views of regions identified in Panels A and B analyzed by (C) histological staining (Saf O/FG) and IHC for (D) Col2, (E) Alk Phos, (F) BMP-6, (G) Ihh, and (H) cathepsin K. Black arrowheads denote cathepsin K-positive osteoclasts. ct, cartilage tube; gp, growth plate-like region; ip, intervertebral pad; oc, ossification center; po, periosteum; rsc, regenerated spinal cord; sc, spinal cord; z, zygapophysial joint. Bar = 100 μm.

This region undergoes a process remarkably similar to endochondral ossification, and the ossified proximal CT is continuous with the original skeleton (Fig. 4B). The hypertrophic chondrocytes of the growth plate-like proximal CT region (Fig. 4C, D) express Alk Phos (Fig. 4E) and BMP-6 (Fig. 4F), and the bordering region adjacent to the growth plate-like zone expresses Ihh (Fig. 4G). Ossification

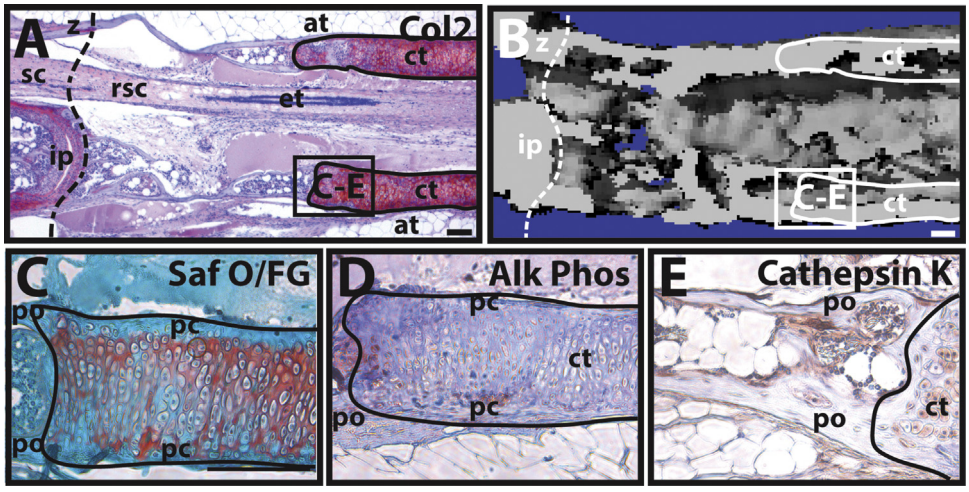

Fig. 5. The growth plate-like organization of the proximal CT breaks down during later stages of regeneration. (A, B) Sagittally sectioned boundary region between original and regenerated tail (70 DPA) analyzed by (A) Col2 IHC and (B) microCT. Solid line denotes the CT boundary. Dashed line denotes boundary between original (left) and regenerated (right) tail. (C-E) Higher magnification views of regions identified in Panels A and B analyzed by (C) histological staining (Saf O/FG) and IHC for (D) Alk Phos, (D) cathepsin K. at, adipose tissue; ct, cartilage tube; et, ependymal tube; ip, intervertebral pad; pc, perichondrium/sub-perichondrium; po, periosteum; rsc, regenerated spinal cord; sc, spinal cord; z, zygapophysial joint. Bar = 100 μm.

centers with cathepsin K-positive osteoclasts form in between the original tail vertebra and the proximal CT (Fig. 4H). Ossification of the proximal CT never extends more than approximately 1 mm distally (Fig. 5A, B) and breaks down during later stages as the growth plate-like region is not renewed as it is converted to bone (Fig. 5C-E). Thus, in the mature (Stage 4) CT, the growth plate-like organization is absent (Fig. 5C), and Alk Phos expression is greatly reduced (Fig. 5D). By 70 DPA, ossification centers shut down as osteoclasts are no longer detected at the boundary between bone and CT (Fig. 5E). Thus, endochondral ossification is limited to the first several millimeters of the proximal CT and never progresses to more distal regions.

The distal CT perichondrium calcifies directly, without undergoing endochondral ossification

Rather than proceeding distally directly from the proximal ossified region, distal CT calcification begins as distinct nodules along the length of the CT perichondrium (Stage 3) (Fig. 6A). Histologically, the distal CT never develops the growth plate organization seen in proximal CT regions (Fig. 6B, C). However, expression of Ihh (Fig. 6D) and Alk Phos (Fig. 6E) do co-localize with distal sites of perichondral calcification. Ihh and Alk Phos are expressed by sub-perichondral chondrocytes adjacent to perichondral regions undergoing calcification. Unlike the proximal CT, distal CT mineralization does not coincide with BMP-6 expression (Fig. 6F), and osteoclasts are not seen at the sites of calcification in the distal CT (Fig. 6G). These differences underlie the two very different mineralization mechanisms controlling proximal vs distal CT mineralization; the proximal CT undergoes endochondral ossification, while the distal CT perichondrium calcifies directly.

Discrete perichondral regions of the distal CT continue to calcify, until the entire inner and outer edges of the perichondrium are completely calcified. Calcification also extends into the sub-perichondral chondrocyte region, but never into more interior CT areas. The last CT region to calcify is a gap (approximately 100 μm) between the proximal and distal calcified region (Fig. S6), reinforcing the fact that the proximal and distal mineralization events are spatially and temporally distinct. Almost a third mineralization event, this gap region calcifies in a process similar to the distal CT; it does not form growth plate-like zones as seen in the proximal CT, instead directly calcifying like the more distal CT.

The mature CT resists further mineralization

The RLT skeleton assumes its mature structure when CT calcification and ossification is complete (Stage 4) and lasts for the life of the regenerate. The proximal CT is ossified to its maximal extent (the most proximal 1 mm), and the distal CT is completely calcified along the inner/outer perichondrium (Fig. 7A). Chondrocytes of the sub-perichondrium express high levels of Ihh (Fig. 7B), while the CT interior expresses BMP-6 (Fig. 7C) and PTHrP (Fig. 7D), and is rich in sulfated glycosaminoglycans (GAGs) (Fig. 7E). Supporting the fact that no additional calcification/ossification takes place, Alk Phos expression is lost (Fig. 7F), and osteoclasts are no longer detected anywhere in the CT (Fig. 7G).

The radial specificity of molecular marker expression and calcification is best appreciated in cross sections of the mature CT (Fig. 7H-M and Fig. S7). Calcification (Fig. 7H) and Ihh expression (Fig. 7I) are limited to the inner and outer perichondrium and sub-perichondrium, while the interior zone of the entire length of the CT consists of a cartilaginous matrix rich in GAG (Fig. 7J) and Col2 (Fig. 9K) with a characteristic mix of proliferative and hypertrophic marker expression. VEGF (Fig. S7A), PTCH1 (Fig. S7B), PTHR1 (Fig. S7C), BMP-6 (Fig. 7L), and BMP-7 (Fig. S7D) are expressed throughout the CT cross section, while Ki67 expression is localized to the middle CT section (Fig. S7E), and PTHrP (Fig. 7M) and RUNX2 (Fig. S7F) are more highly expressed in the inner and outer CT edges adjacent to the perichondrium. BMP-2 (Fig. S7G) is expressed at high levels by the non-CT tissues immediately surrounding the perichondrium. Sox-9 (Fig. S7H) is expressed at low levels by the mature CT.

The mature CT perichondrium contains cartilage "stem/progenitor cells"

The development and calcification of the lizard CT perichondrium in mature regenerates is particularly interesting given the attention stem/progenitor found in the perichondrium and periosteum of mammals have received for their abilities to form cartilage (Arai et al., 2002; Yoshimura et al., 2007). To investigate whether such cells exist in lizard CT perichondrium, CT explants isolated from mature (Stage 4) 70 DPA RLTs were treated with vehicle control (Fig. 8A-D, Fig. S8A-D) or 10 ng/ml TGF-β3 (Fig. 8E-H, Fig. S8E-H), TGF-β1 (Fig. 8I-L, Fig. S8I-L), BMP-2 (Fig. 8M-P,

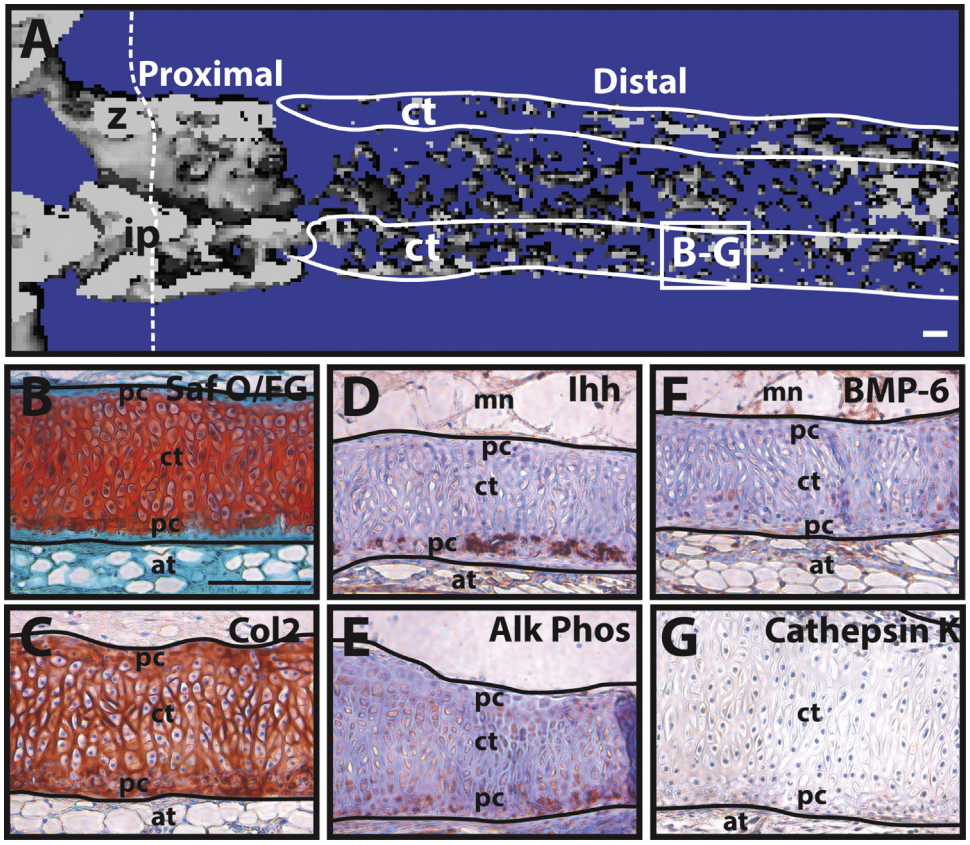

Fig. 6. The distal CT perichondrium mineralizes through direct calcification. (A) Sagittally sectioned microCT scan of a 49 DPA regenerated tail. Solid line denotes the CT. Dashed line denotes boundary between original (left) and regenerated (right) tail. The proximal CT has ossified, while the distal CT begins to calcify at distinct perichondral patches. (B-G) Higher magnification views of regions identified in Panel A analyzed by (B) histology (Saf O/FG) and IHC for (C) Col2, (D) Ihh, (E) Alk Phos, (F) BMP-6, and (G) cathepsin K. at, adipose tissue; ct, cartilage tube; mn, meninges; pc, perichondrium/sub-perichondrium; z, zygapophysial joint. Bar = 100 μm.

Fig. S8M-P) under serum free conditions for 21 days at 37 °C. CTs treated with vehicle control maintain a matrix composed of GAGs (Fig. 8A), Col2 (Fig. 8B), and Col1 (Fig. S8A), a sub-perichondrium that expresses Ihh (Fig. 8C), and an interior that expresses basal levels of Alk Phos (Fig. S8B), Sox-9 (Fig. 8D), RUNX2 (Fig. S8C), and ADAMTS5 (Fig. S8D) throughout explant culture. The CT explants treated with TGF-β3 exhibit significant cartilage growth (Fig. 8E-H, Fig. S8E-H). Nascent cartilage formation coincides with size expansion of a population of Ihh^+, $Alk\ Phos^+$, $RUNX2^+$ perichondral/sub-perichondral cells (Fig. 8G, Fig. S8F-G), which also express Sox-9 (Fig. 8H) and secrete a matrix rich in GAGs (Fig. 8E), Col2 (Fig. 8F), and Col1 (Fig. S8E). New cartilage regions also express ADAMTS5 (Fig. S8H). TGF-β1 treatment also induced cartilage growth (Fig. 8I-J, Fig. S8I) and perichondral cell enlargement (Fig. K-L, Fig. S8J-L), but to a much lesser degree than treatment with TGF-β3. In contrast, BMP-2 treatment does not cause perichondral cell expansion or new matrix formation (Fig. 8M-P, Fig. S8M-P), suggesting the specificity of CT response to growth factors. Thus, rather than being inert, the mature CT is responsive to stimulation by exogenous factors thanks to perichondral "stem/progenitor cells".

Focusing on the perichondral stem cell population, newly formed cartilage regions of TGF-β3-treated explants were examined in greater detail (Fig. 9A-C). In adjacent sections of newly formed cartilage regions analyzed histologically (Saf O/FG, Fig. 9A) and immunohistochemically (Ihh, Fig. 9B; Sox-9, Fig. 9C), the same cells were positive for both Ihh and Sox-9. Histologically, the cytoplasm of these cells stained with Fast Green (Fig. 9A), similar to perichondrium cells and calcified sub-perichondral chondrocytes and unlike chondrocytes of CT interior, again suggesting a perichondral origin. To further investigate the origin of these cells, fate mapping experiments using 5-bromo-2'-deoxyuridin (BrdU) were performed. CT explants were pulsed with BrdU for 48 h in the presence of TGF-β3 and then stimulated with TGF-β3 for 19 days. Proliferative cells were BrdU-immunostained, and adjacent sections were immunostained for markers previously attributed to perichondral/periosteal stem cells, CD166 and CD90 (Arai et al., 2002; Yoshimura et al., 2007). Following pulsing with BrdU, $BrdU^+$ cells were observed in the perichondrium and calcified sub-perichondrium of CT explants (Fig. 9D, E). Following further stumulation with TGF-β3, $BrdU^+$ cells were detected in newly formed cartilage regions (Fig. 9F, H, J). As described above, these cells were Fast Green positive and exhibited significant increases in volume compared to earlier time points (Fig. 9G). Furthermore, the majority of $BrdU^+$ cells also expressed the stem cell markers CD90 (Fig. 9I) and CD166 (Fig. 9K). Taken togeher, these results suggest that "stem/progenitor cells" residing in the perichondrium and calcified sub-perichondral regions of mature CTs respond to TGF stimulation by forming new cartilage regions.

Increases in Ihh expression coincide with both proximal and distal CT calcification events

Immunohistochemistry (IHC) results on mineralization marker expression during both proximal CT ossification and distal CT calcification were confirmed with Western blot (Fig. 10). CTs were isolated from 21–70 DPA RLTs, and total protein samples were extracted from proximal and distal portions. AT 21 DPA, Ihh, Alk Phos, and BMP-6 expression was limited to proximal regions, while both distal and proximal samples expressed VEGF and PTHrP. Proximal CT Ihh, Alk Phos, and BMP-6 expression increases

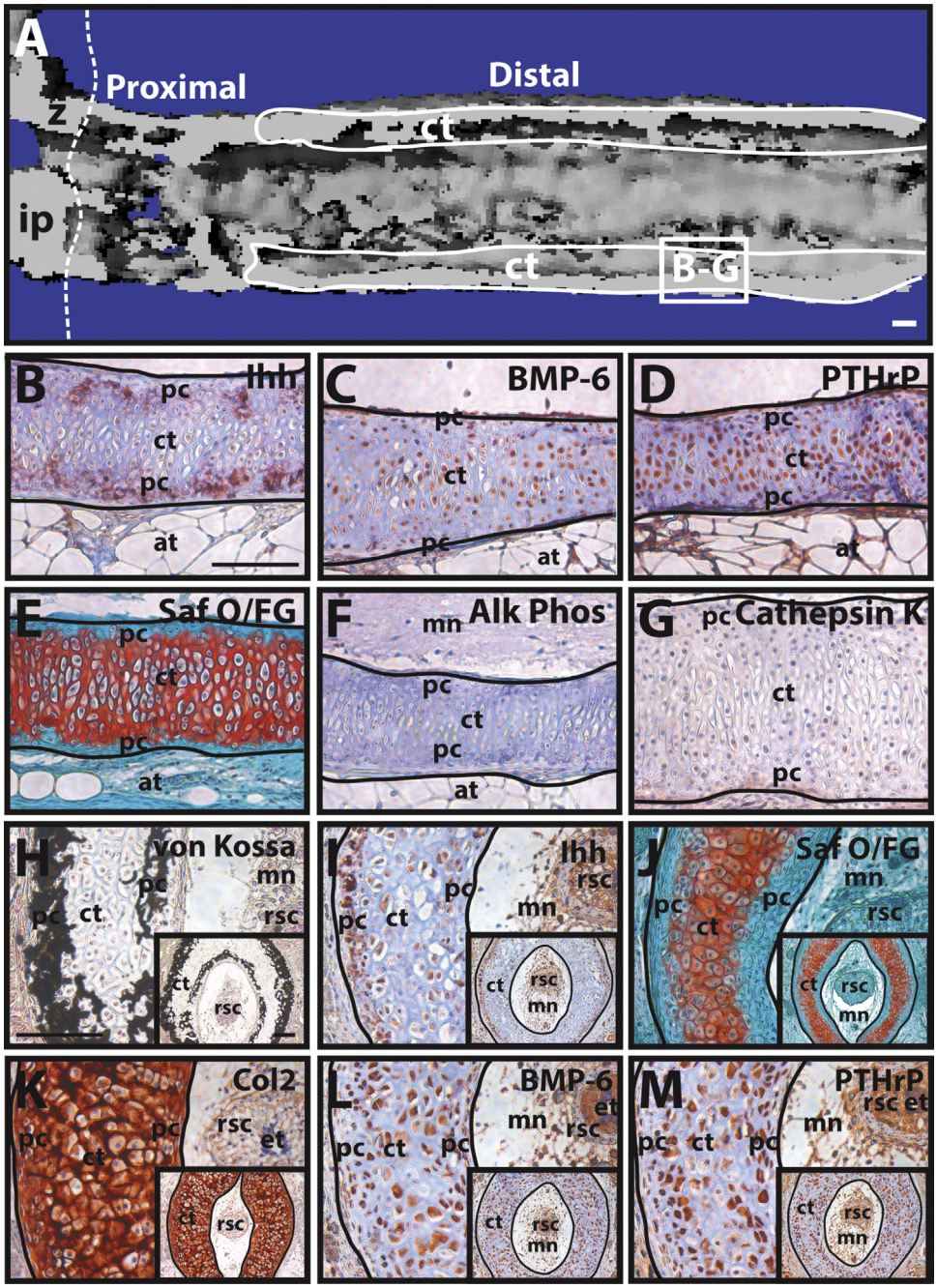

Fig. 7. The distal CT of the mature regenerate is calcified along the perichondrium, while the interior resists further mineralization. (A) Sagittally sectioned microCT scan of a mature regenerated tail (70 DPA). Solid line denotes the CT. Dashed line denotes boundary between original (left) and regenerated (right) tail. Both the proximal and distal RLT regions have attained their mature skeletal structures. (B-G) Higher magnification views of regions identified in Panel A analyzed by (B) Ihh, (C) BMP-6, and (D) PTHrP IHC, (E) histology (Saf O/FG), and IHC for (F) Alk Phos and (G) cathepsin K. (H-M) Cross-sectional views of a mature CT analyzed by histology and IHC for various skeletal development markers: (H) von Kossa, (I) Ihh, (J) Saf O/FG, (K) Col2, (L) BMP-6, (M) PTHrP. adipose tissue; ct, cartilage tube; et, ependymal tube; mn, meninges; pc, perichondrium/sub-perichondrium; rsc, regenerated spinal cord; z, zygapophysial joint. Bar = 100 μm.

during the proximal mineralization event (35 DPA). Conversely, distal CT Ihh and Alk Phos, but not BMP-6, levels increase during distal mineralization (49 DPA). Thus, increases in Ihh and Alk Phos levels coincide with mineralization of both the proximal and distal CT. However, while these regions both mineralize in processes that involve Ihh and Alk Phos, their mechanisms differ; for example, only mineralization of the proximal CT coincided with BMP-6 expression. This may reflect the fact that the proximal CT undergoes endochondral ossification, while the distal CT does not. By 70 DPA, Alk Phos expression is lost in both distal and proximal CT regions, consistent with the absence of further mineralization in the mature regenerate. Ihh, BMP-6, and PTHrP are expressed throughout the CT, again confirming that the mature CT expresses markers of both hypertrophic and proliferating chondrocytes.

A summary of skeletal development within the regenerated lizard tail is presented in Fig. 11, highlighting observations that Ihh expression precedes both ossification of the proximal CT growth plate-like region (Fig. 11A-D) as well as the distal CT perichondrium (Fig. 11E-F). This spatial and temporal linkage of Ihh expression with CT mineralization suggests a role for Ihh in CT

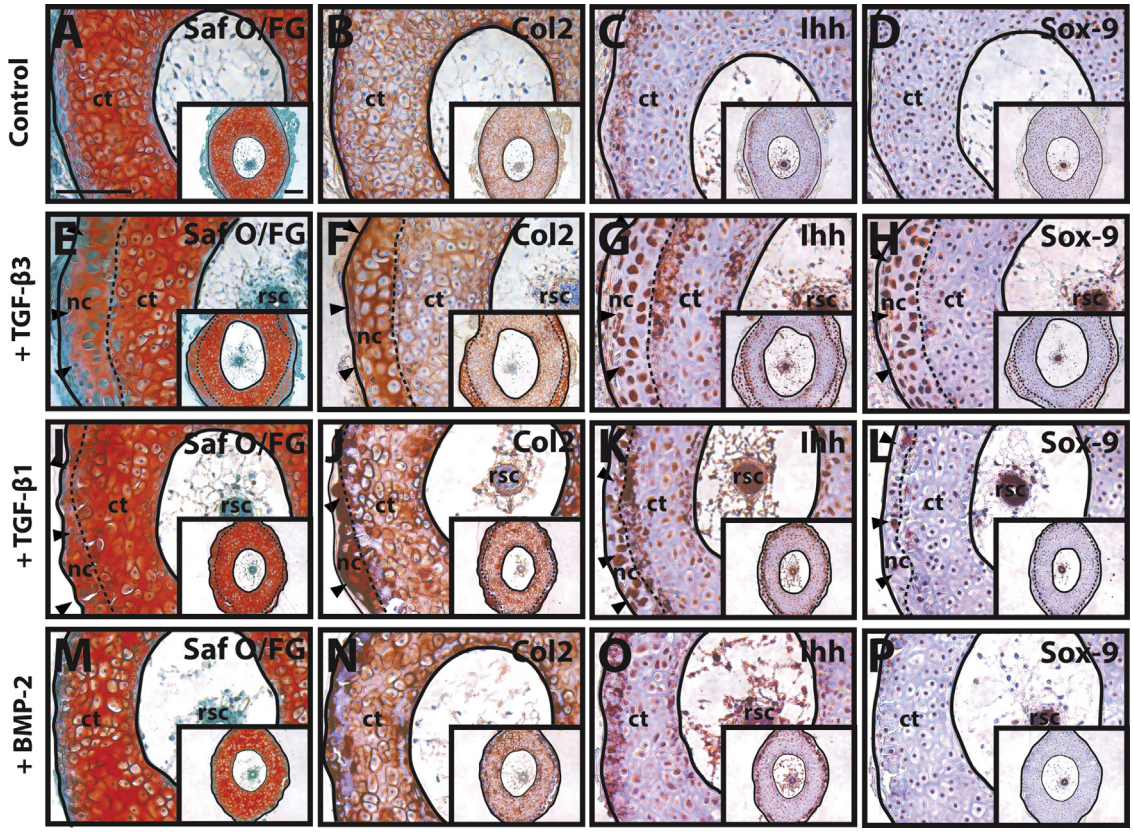

Fig. 8. The mature CT perichondrium responds to stimulation with TGF-β. CT explants isolated from 70 DPA RLTs were treated with (A-D) vehicle control or 10 ng/ml (E-H) TGF-β3, (I-L) TGF-β1, or (M-P) BMP-2 for 21 days and analyzed by histology/IHC. TGF-β-treated, but not BMP-2-treated, explants expanded with new cartilage growth. Solid lines trace CT edges. Dashed lines mark boundary between original and new growth. Arrowheads mark newly formed cartilage rich in GAGs and Col2. TGF-β also causes perichondral stem/progenitor cells to enlarge and express Ihh and Sox-9. ct, cartilage tube; nc, new cartilage; rsc, regenerated spinal cord. Bar = 100 μm.

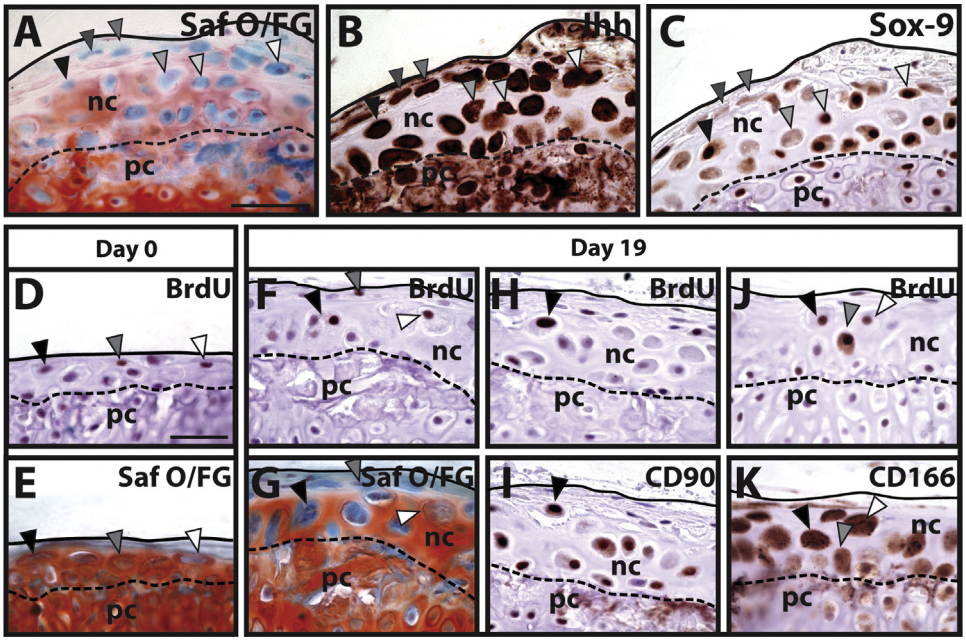

Fig. 9. Stem cells within the CT perichondral region form new cartilage in response to TGF-β stimulation. (A-C) CT explants treated with 10 ng/ml TGF-β3 for 21 days, and adjacent sections of regions of new cartilage growth were analyzed by (A) histology (Saf O/FG), and (B) Ihh and (C) Sox-9 IHC. Arrowheads filled with black, white, or shades of gray mark individual cells recognizable in adjacent sections. Dashed lines mark boundary between original and new growth. Solid lines trace CT edges. (D-K) Fate mapping experiments involving BrdU. CT explants pulsed with BrdU and TGF-β3 for 48 h were treated with TGF-β3 for (D, E) 0 or (F-K) 19 days. New cartilage regions were analyzed by (D, F, H, J) BrdU IHC to identify labeled cells and by (E, G) histology (Saf O/FG) and (I) CD90 and (K) CD166. Adjacent sections are presented in columns, and arrowheads filled with black, white, or gray mark individual cells recognizable in adjacent sections. Dashed lines denote boundaries of calcified perichondral region. Solid lines denote CT boundaries. At Day 0, the region between dashed and solid lines is predominantly perichondrium, while at later time points, this region is mostly made up of newly formed cartilage. nc, new cartilage; pc, perichondrium/sub-perichondrium. Bar = 50 μm.

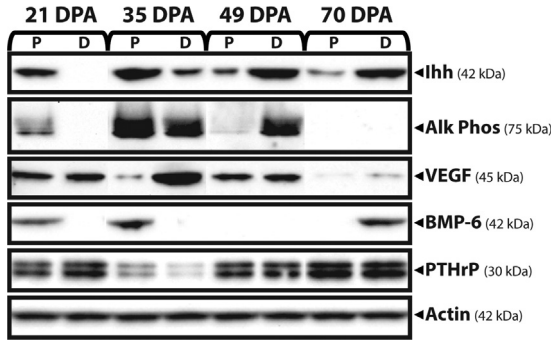

Fig. 10. Western blot-based comparison of proximal vs. distal CT expression of cartilage development markers during lizard tail regeneration. Total protein samples were collected from proximal (P) and distal (D) CT regions isolated from RTLs (21, 35, 49, and 70 DPA), electrophoretically fractionated, and immunoblotted for Ihh, Alk Phos, VEGF, BMP-6, and PTHrP. Actin Western blots were included as loading controls.

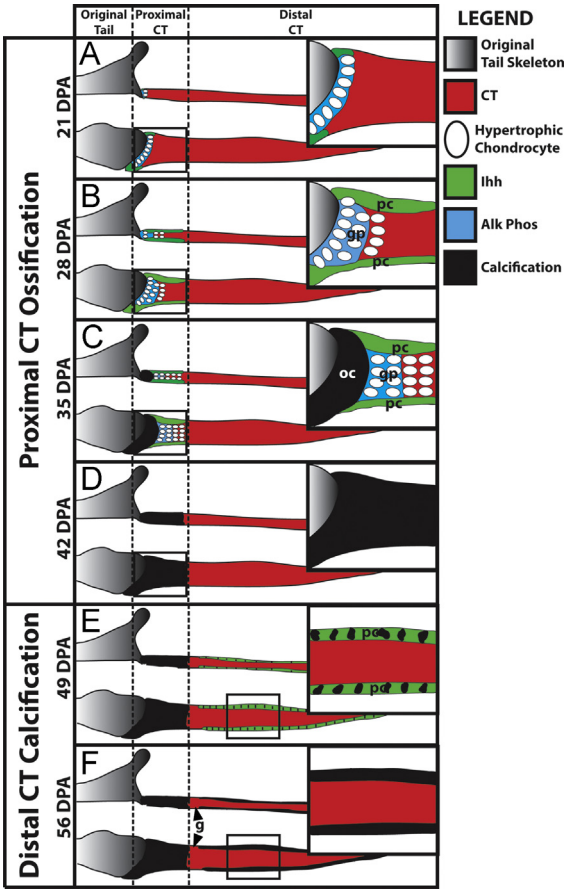

Fig. 11. Summary of regenerated lizard tail skeletal development. (A-F) Sagittally sectioned schematics of a regenerated lizard tail are presented to highlight differences and similarities between the two mineralization events, (A-D) proximal CT ossification and (E-F) calcification of the distal CT sub-perichondrium. (A) By 21 DPA, chondrocytes of the proximal CT in contact with the vertebra of the original tail exhibit hypertrophic morphologies and express Alk Phos (blue). (B) By 28 DPA, the proximal CT has taken on a growth plate-like organization (gp) as the hypertrophic chondrocyte region expands distally to about 1 mm from the terminal vertebra of the original tail. Ihh (green) is expressed by the inner and outer edges of the proximal CT, which develop into perichondrium/periosteum (pc). (C) By 35 PDA, ossification centers form at the proximal CT and the region undergoes endochondral ossification and mineralizes (black). (D) By 42 DPA, the entire proximal CT has been converted to bone, but endochondral ossification of the CT does not proceed into more distal regions. (E) At 49 DPA, the distal CT perichondrium/sub-perichondrium (pc) expresses Ihh and mineralization begins at distinct patches. These patches expand and fuse, and (F) by 56 DPA the CT is calcified along its inner and outer edges. The last region of the distal CT perichondrium to calcify is the gap (g) between proximal ossified CT and the calcified distal perichondrium.

development and provided the rational for the inhibitor studies described below.

Hedgehog signaling is required for proximal CT ossification

Given the critical role Ihh plays in regulating embryonic skeletal development, and the staging results described above showing Ihh expression as a precursor to two distinct CT mineralization events, we hypothesized that inhibiting Ihh would disrupt lizard CT development and mineralization. In the first set of experiments, CTs were isolated from 28 DPA RLTs (before ossification of the proximal CT), analyzed by micro-computed tomography (microCT), and organ cultured for four weeks at 37 °C in the presence of the specific Ihh inhibitor cyclopamine (600 nM) or vehicle control or both cyclopamine and the hedgehog agonist, SAG (40 nM). (Note: 600 nM cyclopamine concentration was validated as not significantly affecting cell viability (Fig. S9)). At the conclusion of the experiment, CT samples were re-evaluated by microCT and analyzed by histology/IHC or western blot. CTs treated with vehicle control develop ossified proximal regions (Fig. 12A), while cyclopamine-treated samples exhibit significantly less proximal calcification (Fig. 12B). Co-treatment with SAG rescues proximal calcification (Fig. 12C). Analysis of the same areas by Col 2 IHC were used to detect CT converted to bone (the Col2-free space in between the regenerated/original tail boundary and the CT) in samples treated with vehicle control (Fig. 12D). These bone regions are drastically reduced in cyclopamine samples (Fig. 12E). Again, treatment with SAG results in the return of ossified CT regions (Fig. 12F). Quantification of microCT measurements of bone volumes in regenerated tail portions confirmed that samples treated with vehicle control and SAG/cyclopamine form more bone than samples treated with cyclopamine alone (Fig. 12G). By histology/IHC, CTs treated with vehicle control exhibit high levels of GAGs (Fig. 12H), periosteal/perichondral Ihh (Fig. 12I), and hypertrophic chondrocytes within a growth plate-like structure that express Alk Phos (Fig. 12J) and BMP-6 (Fig. 12K). Cyclopamine treatment results in decreased GAG expression (Fig. 12L), nearly complete loss of the proximal growth plate-like structure (Fig. 12L), and reduced expression of Ihh (Fig. 12M), Alk Phos (Fig. 12N), and BMP-6 (Fig. 12O). Co-treatment with SAG causes partial rescue of GAG (Fig. 12P), Ihh (Fig. 12Q), Alk Phos (Fig. 12R), and BMP-6 (Fig. 12S) expression; however, Ihh, ALK Phos, and BMP-6 appear less organized in the SAG samples than in vehicle control samples. Cyclopamine-induced decreases in hypertrophy markers and the ability of SAG to partially rescue their expression were confirmed with Western blot (Fig. 12T).

Hedgehog signaling is required for distal CT calcification

In this set of experiments, CTs isolated from 42 DPA RLTs (before calcification of the distal CT perichondrium) were cultured in the presence of 600 nM cyclopamine, vehicle control, or both cyclopamine and SAG (40 nM) for four weeks at 37 °C. CTs treated with vehicle control develop patches of calcification in the perichondrium of distal regions (Fig. 13A). Cyclopamine treatment results in significant reduction in distal CT calcification as the formation of perichondral punctate regions of calcification is inhibited (Fig. 13B). Co-treatment of SAG with cyclopamine rescues calcification (Fig. 13C). Quantification of distal CT bone volume by microCT confirmed that vehicle control and SAG/cyclopamine co-treated samples are significantly more calcified than samples treated with cyclopamine alone (Fig. 13D). Control CT explants treated with vehicle control develop perichondral patches that are positive for Ihh (Fig. 13E) and Alk Phos (Fig. 13F), while interior regions of control samples express PTHrP (Fig. 13G). Cyclopamine

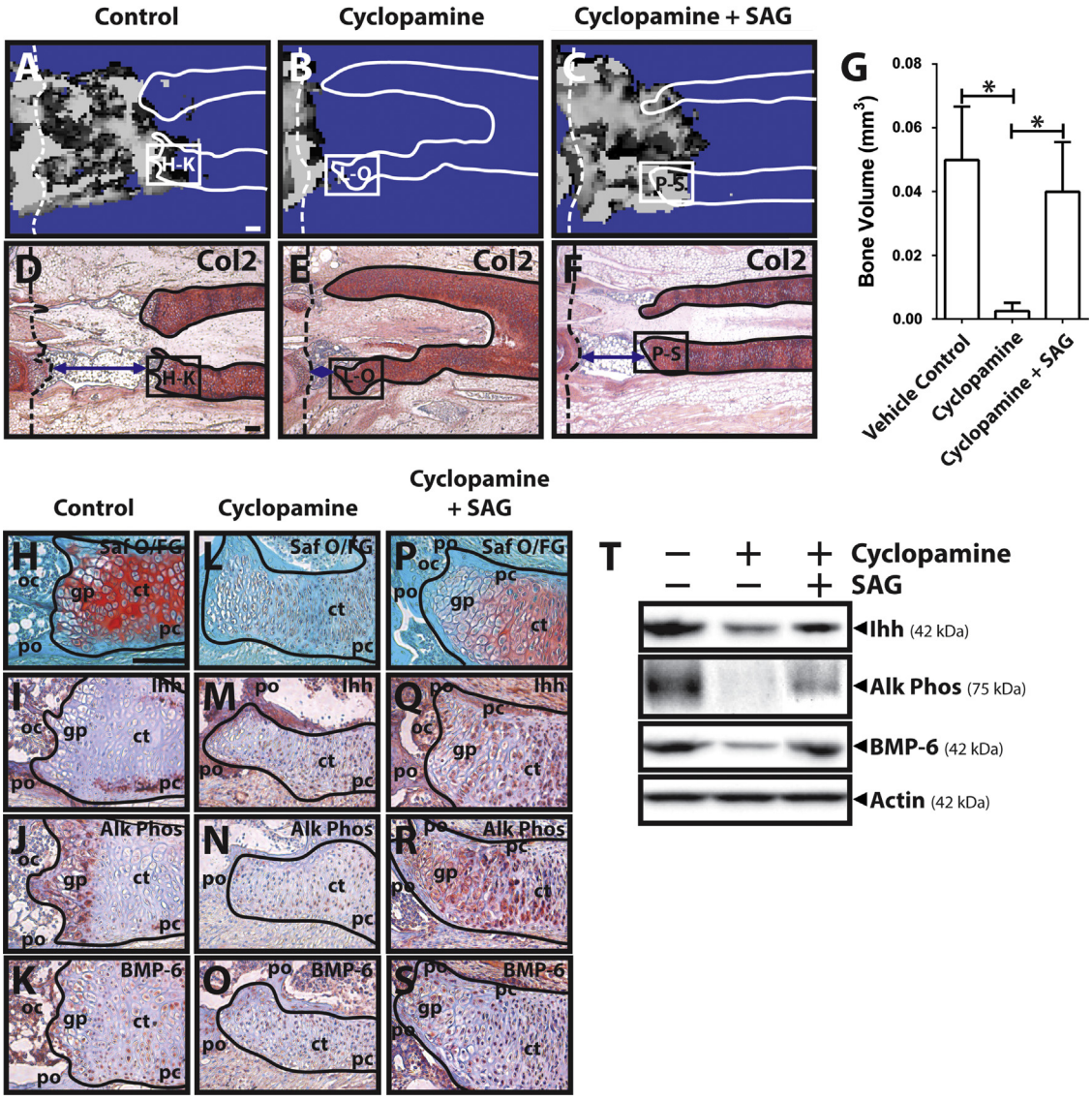

Fig. 12. Cyclopamine treatment inhibits proximal CT ossification. CT explants collected from 28 DPA RLTs were treated with vehicle control, 600 nM cyclopamine, or co-treated with cyclopamine and 40 nM SAG for 28 days. (A-F) Sagittally sectioned boundary regions between original and regenerated tail of explants treated with vehicle control, cyclopamine, or cyclopamine and SAG were analyzed by (A-C) microCT and (D-F) Col2 IHC. Solid line denotes the CT boundary. Dashed line denotes boundary between original (left) and regenerated (right) tail. Blue double-arrowed lines in Panels D-F span the CT lengths that have undergone endochondral ossification. (G) MicroCT comparison of bone volume of regenerated tail portions between CT explants treated with vehicle control, cyclopamine, or cyclopamine and SAG ($n=3$). *, $p<0.05$ (H-S) Higher magnification views of region identified in Panels A-F analyzed by (H, L, P) histology (Saf O/FG) and IHC for (I, M, Q) Ihh, (J, N, R) Alk Phos, (K, O, S) BMP-6. (T) Western blot analysis of Ihh, Alk Phos, and BMP-6 expression in proximal CTs isolated from explants treated with vehicle control, cyclopamine, or cyclopamine and SAG. ct, cartilage tube; gp, growth plate-like region; oc, ossification center; pc, perichondrium/sub-perichondrium. Bar = 100 μm.

treatment significantly decreases perichondral expression of Ihh (Fig. 13H), Alk Phos (Fig. 13I) and overall CT expression of PTHrP (Fig. 13J). Co-treatment with SAG partially rescues expression of Ihh (Fig. 13K), Alk Phos (Fig. 13L), and PTHrP (Fig. 13M). However, Ihh and Alk Phos expression rescued by SAG treatment is more cellular and not as tightly associated with the perichondrium than that which is observed in vehicle control samples. These changes in marker expression were confirmed by Western blot (Fig. 13N).

Discussion

Lizard tail regeneration has a long, yet patchy, history of scientific study. The ability of lizards to regenerate their tails was known to Aristotle in the fourth century B.C., but more detailed observations were not performed until the late seventeenth century with the discovery that the skeleton of the regenerate consists of cartilage and not of new bony vertebrae (see Bellairs and Bryant, 1985). Modern scientific interest in lizard tail regeneration was largely pioneered by two scientists, Drs. Sidney Simpson, JR., and Lorenzo Alibardi (Simpson, 1964; Simpson and Cox, 1967; Alibardi and Meyer-Rochow, 1989). Work with lizard tail regeneration has since grown steadily, and recently a handful of groups began focusing on this research area (McLean and Vickaryous, 2011; Wang et al., 2011; Delorme et al., 2012; Fisher et al., 2012; Dong et al., 2013; Eckalbar et al., 2013; Hutchins et al., 2014). Our study described here presents several first-time observations that should enhance our understanding of this unique biological phenomenon. Specifically, this study presents detailed analyses of the various stages of RLT skeletal development with high-resolution microCT imaging, links mineralization data with analyses of skeletal developmental markers, and correlates RLT cartilage development and mineralization with cartilage maturation markers.

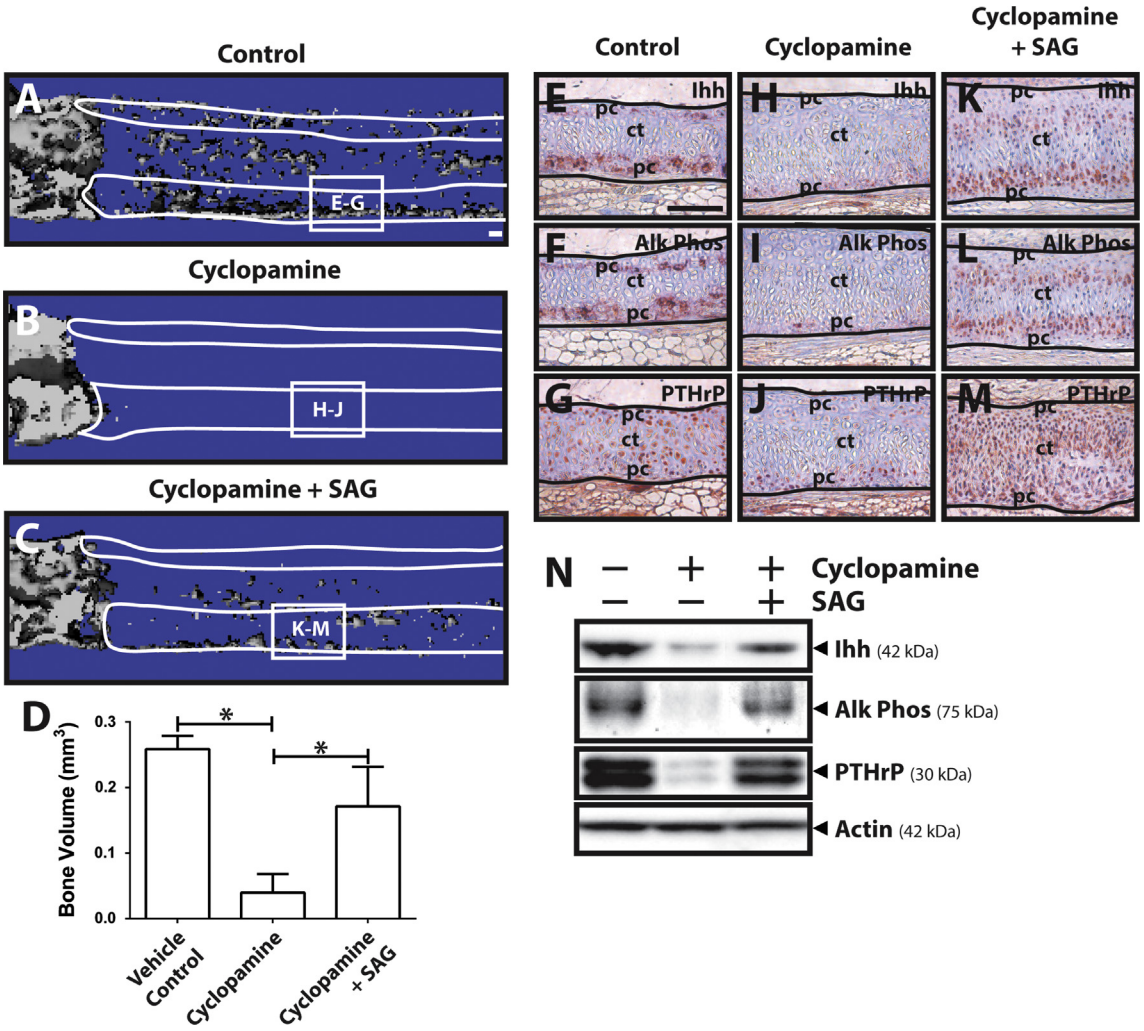

Fig. 13. Cyclopamine treatment inhibits distal CT calcification. CT explants collected from 42 DPA RLTs were treated with vehicle control, 600 nM cyclopamine, or co-treated with cyclopamine and 40 nM SAG for 28 days. (A-C) Sagittally sectioned microCT scans of regenerated tail explants treated with (A) vehicle control, (B) cyclopamine, or (C) cyclopamine and SAG. Solid line denotes the CT boundary. (D) MicroCT comparison of bone volume of regenerated tail portions between RLT explants treated with vehicle control, cyclopamine, or cyclopamine and SAG ($n=3$). *, $p<0.05$ (E-M) Higher magnification views of region identified in Panels A-C analyzed by IHC for (E, H, K) Ihh, (F, I, L) Alk Phos, (G, J, M) PTHrP. (T) Western blot analysis of Ihh, Alk Phos, and PTHrP expression in proximal CTs isolated from RLT explants treated with vehicle control, cyclopamine, or cyclopamine and SAG. ct, cartilage tube; pc, perichondrium/sub-perichondrium. Bar = 100 μm.

Our findings describe the structural and biological characteristics of the boundary between the original and regenerated lizard skeletons, the growth plate-like region, and endochondral ossification of the proximal CT. The transient nature of this regenerative phenomenon, both in terms of time and location, within the RLT has proven difficult to study in the past. Only the most proximal first millimeter or so of the CT undergoes endochondral ossification of growth-plate like structures in a process almost completely limited to a single, distinct stage of lizard tail regeneration - Stage 2 as described here, corresponding to approximately 4–6 weeks post autotomy. This finding may be controversial because conventional theories dictate that the lizard tail is completely boneless, i.e., that no portion of the cartilage tube ossifies, and many previous studies assumed that what we have identified as ossified CT was part of the terminal vertebra of the original tail-stump. Our study details bone remodeling activities that take place in the terminal hemi-vertebra prior to regeneration, thus enabling us to unequivocally distinguish between the original and regenerated tail portions. This analysis has allowed us to identify the specific regions of the CT that do, in fact, ossify.

Our study also analyzed the distal CT calcification process by high resolution microCT. Previous studies described calcification of the inner and outer edges of the CT (Alibardi, 2010). Many of these studies were performed on mature regenerates, when the CT perichondrium is completely calcified. We considered the CT at various stages during the process of calcification, and, in doing so, we were able to detect the interesting and unusual patchy pattern that defines early distal CT calcification.

The novel aspect of our study is the investigation of the role of Ihh in lizard tail regeneration using the inhibitor cyclopamine and the agonist, SAG. Two distinct mineralization events were identified during lizard CT development, and both of these mineralization processes were correlated with Ihh expression. Cyclopamine has been used to investigate the role of hedgehog signaling in urodele limb and tail regeneration (Schnapp et al., 2005). However, in these studies, cyclopamine treatment was administered during the earliest stages of regeneration, typically during chondrogenic differentiation. Ours is one of the few studies to investigate the role of Ihh in later stages of development in adult regeneration, in this case lizard tail regeneration. Again, having staging information of RLT skeletal development at hand has allowed us to administer treatment at specific times to investigate specific mineralization events. In the cases of both mineralization events, cyclopamine treatment resulted in loss of Ihh expression as well as inhibition of calcification. In the embryonic growth plate,

such as during endochondral ossification in the limb, Ihh signals through PTCH1 to increase expression of BMPs, which feed back to increase Ihh expression and signaling (Minina et al., 2001). Thus, we hypothesize that during CT development, Ihh operates in concert with BMP signaling to maintain both its own expression as well as environments supportive of ossification/mineralization, and that inhibition with cyclopamine interferes with this feedback loop, resulting in loss of Ihh expression. However, there also appears to be deviation between growth plate and proximal CT Ihh signaling. In the embryonic growth plate, Ihh signals through proliferative chondrocytes and PTHrP to inhibit hypertrophy (Minina et al., 2001), an effect reversed by cyclopamine treatment, which is opposite to what we observed in the proximal CT growth plate-like zone. Thus, Ihh may be acting independently of PTHrP in regulating hypertrophy and ossification within the proximal CT, perhaps due to the unique geometry of the lizard CT where proliferating chondrocytes are so removed spatially from Ihh-expressing regions. Future studies will be aimed at elucidating the specific roles of BMPs and PTHrP in CT development.

Experiments involving explant culture of lizard CTs are carried out here to identify stem/progenitor-like cells within the perichondrium of mature CTs. Stem/progenitor cells capable of forming cartilage have been reported to reside in the perichondrium and periosteum of mammals (Arai et al., 2002; Yoshimura et al., 2007), and our study describes similar cells in lizards, and specifically in an adult regenerated tissue, that express the perichondral/periosteal stem cell markers CD166 and CD90, as well as the sub-perichondral/pre-hypertrophy marker Ihh. Upon stimulation with TGF-β, these cells proliferate, and increase their expression of the chondrocyte marker Sox-9. Thus, CT perichondral stem cells retain markers indicative of their origin (Ihh, CD166, CD90) as they up-regulate Sox-9 and synthesize new cartilage matrix in response to TGF-β.

Our findings, therefore, represent important progress toward understanding lizard skeletal regeneration and future studies will continue along this path. For example, future work will focus on answering the question as to why endochondral ossification is limited to the proximal CT and does not progress more distally. We hypothesize that factors released by the original, but not regenerated, tail skeleton induce formation of the proximal growth plate-like region. Future studies will also compare what we have observed in the lizard tail with what happens during regeneration of the salamander tail, which undergoes perichondral/periosteal segmentation, to determine how the two processes differ and whether Ihh is involved. Furthermore, it did not escape our notice that proximal CT ossification stops at the same general location of the original fracture plane, suggesting the existence of some type of spatial memory cues during embryonic development of the original tail vertebrae. It will be interesting to investigate whether embryonic development and specification of the fracture plane exhibits the same unusual pattern of Ihh expression observed in the developing CT

Also of note, the skeletal marker analysis performed as part of this study yielded several counterintuitive yet interesting findings. For example, we were unable to detect Col10 and MMP-13, classic markers of cartilage hypertrophy, at any point during CT development, including the proximal growth-plate like zone. Neither Col10 nor MMP-13 was detectable in lizard CT samples by Western blot and IHC compared to positive controls (Figs. S10, S12), including embryonic lizard growth plates. Thus, as of now, we must consider the possibility that endochondral ossification that occurs at the proximal CT proceeds without Col10 and/or MMP-13. This is an interesting concept, as it may represent an important difference between embryonic and regenerative endochondral ossification, and future studies will be aimed toward elucidating the roles of Col10 and MMP-13 in CT development. Furthermore, results from Col2 and Col1 expression analyses suggest that Col1 and Col2 are co-expressed by the CT during all stages of development. This is unusual because the CT has typically been described as hyaline cartilage (Cox, 1969; Alibardi, 2010; Fisher et al., 2012), which does not normally express Col1. Thus, it may be more accurate to describe the CT matrix composition as similar to growth plate cartilage. To demonstrate this, lizard growth plate samples were analyzed for Col1 and Col2 expression (Fig. S11). Col1 and Col2 were co-expressed in the pre-hypertrophy, but not proliferative, zones of lizard growth plate. Thus, these results suggest that the matrix composition of CTs is similar to that of pre-hypertrophic growth plate cartilage.

In conclusion, our findings present critical, anatomical, histological, cellular and molecular milestones in lizard tail skeletal remodeling and regeneration, including autotomy, ablation, CT formation, proximal CT ossification, and calcification of the distal CT. We have identified two distinct mineralization events that, despite spatial, temporal, and mechanistic differences, both involve Ihh. We have also studied the mature regenerated tail, finding it resistant to mineralization and yet responsive to specific growth factors and capable of generating new cartilage. The regenerated lizard tail thus represents an interesting and useful experimental model of cartilage regeneration.

Materials and methods

RLT and CT isolation

Fresh RLTs (*Anolis sagrei*) were obtained from reptile supply companies (Tails 'n More Pet Services, Underground Reptiles) and cut into sections. The regenerated/original tail boundaries were identified by changes in scalation and coloration (Fig. S13). RLTs were cut approximately 0.5 cm distal and proximal of the boundaries. The remaining RLT was cut into sections approximately 1 cm in length. To isolate CTs, RLT slices were dissected with tungsten needles, and collected CTs were either organ cultured, used to isolate lizard chondrocytes or immediately frozen in liquid nitrogen for protein isolation. RLT pieces, including regenerated/original tail boundaries, to be analyzed by microCT and histology/immunohistochemistry (IHC) were fixed overnight in 4% paraformaldehyde (Electron Microscopy Sciences), washed with phosphate-buffered saline (PBS) (Life Technologies), and stored in 70% ethanol.

Lizard CT organ culture

CT explants were cultured at 37 °C in chicken collagen type 1 (Col1) gels (EMD Millipore) in Ham's F12 medium (Life Technologies) containing 50 μg/ml ascorbate (Sigma-Aldrich), 40 μg/ml L-proline (Sigma-Aldrich), 0.1 μM dexamethasone (Sigma-Aldrich), and 1X insulin-transferrin-selenium (ITS) supplement (Life Technologies). For cyclopamine and experiments, CT explants were cultured in 1:1 DMEM/F12 (Life Technologies), 1.1 mM $CaCl_2$ (Sigma-Aldrich), 1% glucose (Sigma-Aldrich), 0.25 mM β-glycerophosphate (Sigma-Aldrich), 0.3 mg/ml glutamine (Sigma-Aldrich), 25 μg/ml ascorbate, ITS, containing 600 nM cyclopamine (LC Laboratories) or vehicle control (45% (2-Hydroxypropyl)-β-cyclodextrin) (Sigma-Aldrich). To rescue hedgehog signaling from inhibition by cyclopamine, CT explants media was supplemented with 40 nM of the smoothened agonist SAG (N-Methyl-N′-(3-pyridinylbenzyl)-N'-(3-chlorobenzo[b] thiophene-2-carbonyl)-1,4-diaminocyclohexane) (Stem RD).

Micro computed tomography (microCT)

Samples were immersed in PBS and scanned with a vivaCT 40 (Scanco Medical, Switzerland) (Resolution, 19 μm; Energy, 70 kVp;

Current, 114 μA). For staging experiments, microCT scans were converted to 3D reconstructions. For cyclopamine experiments, bone volume measurements were based on scans of samples before and after four weeks of treatment with 600 nM cyclopamine or vehicle control. Changes in calcification were calculated by subtracting initial from week 4 bone volume measurements.

Statistics

Bone volume measurements are expressed as the mean ± SD, and significant differences between control and experimental conditions were determined by two-tailed Student's t-tests.

Histology

RLT pieces, except those to be von Kossa stained, were decalcified in Immunocal (Decal) for 72 h, dehydrated by graded ethanol washes, cleared in xylene, embedded in paraffin, sectioned at 7 μm thickness, mounted on glass slides, and rehydrated. Non-decalcified samples were embedded in glycol methacrylate (GMA) (Technovit 7100 Embedding Kit) according to the manufacturer's instructions, sectioned at 3 μm thickness with a tungsten-carbide knife (Delaware Diamond Knives), and mounted on glass slides. For hematoxylin and eosin staining (H&E), slides were stained with hematoxylin, Gill No. 2, (Sigma-Aldrich) for 20 min and eosin for 1 min. For Movat's pentachrome stain, slides were stained with Alcian blue (American MasterTech) for 20 min, hematoxylin for 15 min, crocein scarlet-acid fuchsin (American MasterTech) for 2 min, 5% aqueous phosphotungstic acid (American MasterTech) for 5 min, and alcoholic safran solution (American MasterTech) for 15 min. For Safranin O/Fast Green FCF (Saf O/FG) staining, samples were stained with hematoxylin for 5 min, 0.02% Fast Green FCF (Electron Microscopy Sciences) for 5 min, rinsed with 1% acetic acid and stained with 0.2% Safranin O (Electron Microscopy Sciences) for 10 min. For von Kossa staining, samples were incubated with 1% silver nitrate (Sigma-Aldrich) under UV light for 30 min, then 5% sodium thiosulfate (Sigma-Aldrich) for 5 min.

Immunohistochemistry (IHC)

Enzymatic or heat-mediated antigen retrieval was performed with either 1 mg/ml chondroitinase (Sigma-Aldrich) and 5 mg/ml hyaluronidase (Sigma-Aldrich) for 30 min at 37 °C or with sodium citrate buffer, pH 6.0, (eBioscience) for 20 min at 95 °C, respectively. Endogenous peroxidase was blocked with 3% H_2O_2 (Sigma-Aldrich) in methanol for 10 min, and nonspecific binding was suppressed with 1% horse serum (Vector Labs) in PBS for 45 min. Following antigen retrieval and blocking, samples were incubated with primary antibodies against cathepsin K, Col2, Col1, Alk Phos, Ihh, PTHrP, BMP-6, VEGF, Col10, sox-9, RUNX2, BMP-2, PTHR1, MMP-13, BMP-7, Ki67, PTCH1, ADAMTS5, CD166, or CD90 overnight at 4 °C (please see Table S1 for IHC primary antibody information), followed by 30 min with biotinylated secondary antibodies. Staining was developed by incubating samples with horseradish peroxidase (HRP)-conjugated streptavidin and treating with the Vector® NovaRED™ peroxidase substrate, and counterstained with hematoxylin (Vector Labs). Following staining, histology and IHC, samples were dehydrated, mounted, and coverslipped, and images were captured with an Olympus CKX41 microscope outfitted with a Leica DFC 3200 camera.

Protein sample collection and Western blot

Lizard CTs were collected into RIPA buffer (EMD Millipore), homogenized through sonication, and centrifuged (12000 × g for 10 min) to remove insoluble fraction. To isolate proximal and distal CT samples, the proximal 2 mm of the CTs were dissected from the remaining distal CT portion, and each was solubilized in RIPA buffer. Solubilized protein samples (15 μg) were subjected to reducing SDS-polyacrylamide gel electrophoresis, transferred to polyvinylidene fluoride membranes (EMD Millipore), and probed overnight with primary antibodies against Ihh, Alk Phos, VEGF, BMP-6, PTHrP, PTHR1, Col10, RUNX2, MMP-13, or β-actin (please see Table S2 for Western blot primary antibody information and Fig. S12 for antibody validation), incubated with HRP-conjugated secondary antibodies (Thermo Scientific), followed by chemiluminescent HRP substrate (Thermo Scientific), and imaged with a Fotodyne/Analyst FX CCD camera system.

5-Bromo-2'-deoxyuridin (BrdU) labeling

Lizard CT explants embedded in chicken collagen type 1 gels were treated with 1 μM BrdU (Life Technologies) and 10 ng/ml TGF-β3 for 48 h, washed with PBS, and treated with 10 ng/ml TGF-β3 in the absence of BrdU for an additional 19 days. Explants were then processed for histology, and $BrdU^+$ cells were detected through IHC using anti-BrdU primary antibody (Abcam ab6326).

Tissue viability

Lizard explant viabilities were measured with the CellTiter 96® AQueous One Solution Cell Proliferation Assay (MTS) (Promega) according to the manufacturer's instructions. In reporting viability results, assay measurements were normalized to wet tissue weight to account for differences in cell number.

Acknowledgments

This project was supported by the Commonwealth of Pennsylvania Department of Health (SAP 4100050913).

Appendix A. Supporting information

Supplementary data associated with this article can be found in the online version at http://dx.doi.org/10.1016/j.ydbio.2014.12.036.

References

Adams, S.L., Cohen, A.J., Lassova, L., 2007. Integration of signaling pathways regulating chondrocyte differenatiation during endochondral bone formation. J. Cell Physiol. 213, 635–641.

Alibardi, L., 2010. Morphological and cellular aspects of tail and limb regeneration in lizards. A model system with implications for tissue regeneration in mammals. Adv. Anat. Embryol. Cell Biol. 207, 1–109 (iii, v-x).

Alibardi, L., Meyer-Rochow, V.B., 1989. Comparative fine structure of the axial skeleton inside the regenerated tail of some lizard species and the tuatara (Sphenodon punctatus). Gegenbaurs Morphol. Jahrb. 135, 705–716.

Anderson, H.C., Sipe, J.B., Hessle, L., Dhanyamraju, R., Atti, E., Camacho, N.P., Millan, J.L., 2004. Impaired calcification around matrix vesicles of growth plate and bone in alkaline phosphatase-deficient mice. Am. J. Pathol. 164, 841–847.

Arai, F., Ohneda, O., Miyamoto, T., Zhang, X.Q., Suda, T., 2002. Mesenchymal stem cells in perichondrium express activated leukocyte cell adhesion molecule and participate in bone marrow formation. J. Exp. Med. 195, 1549–1563.

Bellairs, A.D., Bryant, S.V., 1985. Autotomy and regeneration in reptiles (*Development B*). In: Gans, C., Billet, F. (Eds.), The Biology Of The Reptilia, *Volume* 15. John Wiley & Sons, Inc., New York, pp. 303–410.

Chung, U., Schipani, E., McMahon, A., Kronenberg, H.M., 2001. Indian hedgehog couples chondrogenesis to osteogenesis in endochondral bone development. J. Clin. Invest. 107, 295–304.

Cox, P., 1969. Some aspects of tail regeneration in the lizard, *Anolis carolinensis*. I. A description based on histology and autoradiography. J. Exp. Zool. 171, 127–150.

DeLise, A.M., Fischer, L., Tuan, R.S., 2000. Cellular interactions and signaling in cartilage development. Osteoarthr. Cartil. 8, 309–334.

Delorme, S.L., Lungu, I.M., Vickaryous, M.K., 2012. Scar-free wound healing and regeneration following tail loss in the leopard gecko, eublepharis macularius. Anat. Rec. 295, 1575–1595.

Dirckx, N., Van Hul, M., Maes, C., 2013. Osteoblast recruitment to sited of bone formation in skeletal development, homeostasis, and regeneration. Birth Defects Res. Part C 99, 170–191.
Dong, Y., Gu, Y., Huan, Y., Wang, Y., Liu, Y., Liu, M., Ding, F., Gu, X., Wang, Y., 2013. HMGB1 protein does not mediate the inflammatory response in spontaneous spinal cord regeneration: a hint for CNS regeneration. J. Biol.l Chem. 288, 18204–18218.
Eckalbar, W.L., Hutchins, E.D., Markov, G.J., Allen, A.N., Corneveaux, J.J., Lindblad-Toh, K., Di Palma, F., Alfoldi, J., Huentelman, M.J., Kusumi, K., 2013. Genome reannotation of the lizard Anolis carolinensis based on 14 adult and embryonic deep transcriptomes. BMC Genomics 14, 49.
Fisher, R.E., Geiger, L.A., Stroik, L.K., Hutchins, E.D., George, R.M., Denardo, D.F., Kusumi, K., Rawls, J.A., Wilson-Rawls, J., 2012. A histological comparison of the original and regenerated tail in the green anole, Anolis carolinensis. Anat. Rec. 295, 1609–1619.
Hutchins, E.D., Markov, G.J., Eckalbar, W.L., George, R.M., King, J.M., Tokuyama, M.A., Geiger, L.A., Emmert, N., Ammar, M.J., Allen, A.N., Siniard, A.L., Corneveaux, J.J., Fisher, R.E., Wade, J., DeNardo, D.F., Rawls, J.A., Huentelman, M.J., Wilson-Rawls, J., Kusumi, K., 2014. Transcriptomic analysis of tail regeneration in the lizard Anolis carolinensis reveals activation of conserved vertebrate developmental and repair Mechanisms. PLoS One, 9. http://dx.doi.org/10.1371/journal.pone.0105004.
Iten, L.E., Bryant, S.V., 1976. Stages of tail regeneration in the adult newt, Notophthalmus viridescens. J. Exp. Zool. 196, 283–292.
Kronenberg, H.M., 2003. Developmental regulation of the growth plate. Nature 423, 332–336.
Kronenberg, H.M., 2006. PTHrP and skeletal development. Ann. N. Y. Acad. Sci. 1068, 1–13.
Lanske, B., Kronenberg, H.M., 1998. Parathyroid hormone-related peptide (PTHrP) and parathyroid hormone (PTH)/PTHrP receptor. Crit. Rev. Euk. Gene Exp. 8, 297–320.
Lee, K., Lanske, B., Karaplis, A.C., Deeds, J.D., Kohno, H., Nissenson, R.A., Kronenberg, H.M., Segre, G.V., 1996. Parathyroid hormone-related peptide delays terminal differentiation of chondrocytes during endochondral bone development. Endocrinology 137, 5109–5118.
Lehoczky, J., Robert, B., Tabin, C., 2011. Mouse digit tip regeneration is mediated by fate-restricted progenitor cells. Proc. Natl. Acad. Sci. USA 108, 20609–20614.
Mackie, E.J., Ahmed, Y.A., Tatarczuch, L., Chen, K.S., Mirams, M., 2008. Endochondral ossification: how cartilage is converted into bone in the developing skeleton. Int. J. Biochem. Cell Biol. 40, 46–62.
Man-Ger Sun, M., Beier, F., 2014. Chondrocyte hypertrophy in skeletal development, growth, and disease. Birth Defects Res. Part C 102, 74–82.
McLean, K.E., Vickaryous, M.K., 2011. A novel amniote model of epimorphic regeneration: the leopard gecko, Eublepharis macularius. BMC Dev. Biol. 11, 50–74.
Minina, E., Wenzel, H.M., Kreschel, C., Karp, S., Gaffield, W., McMahon, A.P., Vortkamp, A., 2001. BMP and Ihh/PTHrP signaling interact to coordinate chondrocyte proliferation and differentation. Development 128, 4523–4534.
Ohba, S., Chung, U., 2014. PTHrP action on skeletal development: a key for the controlled growth of endochondral bones. Clin. Rev. Bone Miner. Metab. 12, 130–141.
Schnapp, E., Kragl, M., Rubin, L., Tanaka, E.M., 2005. Hedgehog signaling controls dorsoventral patterning, blastema cell proliferation and cartilage induction during axolotl tail regeneration. Development 132, 3243–3253.
Simpson Jr., S.B., 1964. Analysis of tail regeneration in the lizard lygosoma laterale. I. Initiation of regeneration and cartilage differentiation: the role of Ependyma. J. Morphol. 114, 425–435.
Simpson Jr.,, S.B., Cox, P.G., 1967. Vertebrate regeneration system: culture in vitro. Science 157, 1330–1332.
St-Jacques, B., Hammerschmidt, M., McMahon, A.P., 1999. Indian hedgehog signaling regulates proliferation and differentiation of chondrocytes and is essential for bone formation. Genes Dev. 13, 2072–2086.
Tsang, K.Y., Tsang, S.W., Chan, D., Cheah, K.S., 2014. The chondrocytic journey in endochondral done growth and skeletal dysplasia. Birth Defects Res. Part C 102, 52–73.
van der Eerden, B.C., Karperien, M., Wit, J.M., 2003. Systemic and local regulation of the growth plate. Endocr. Rev. 24, 782–801.
Vortkamp, A., Lee, K., Lanske, B., Segre, G.V., Kronenberg, H.M., Tabin, C.J., 1996. Regulation of rate of cartilage differentiation by Indian hedgehog and PTH-related protein. Science 273, 613–622.
Wang, Y., Wang, R., Jiang, S., Zhou, W., Liu, Y., Wang, Y., Gu, Q., Gu, Y., Dong, Y., Liu, M., et al., 2011. Gecko CD59 is implicated in proximodistal identity during tail regeneration. PloS One 6, e17878.
Yoshimura, H., Muneta, T., Nimura, A., Yokoyama, A., Koga, H., Sekiya, I., 2007. Comparison of rat mesenchymal stem cells derived from bone marrow, synovium, periosteum, adipose tissue, and muscle. Cell Tissue Res. 327, 449–462.
Zelzer, E., Glotzer, D.J., Hartmann, C., Thomas, D., Fukai, N., Soker, S., Olsen, B.R., 2001. Tissue specific regulation of VEGF expression during bone development requires Cbfa1/Runx2. Mech. Dev. 106, 97–106.